

The Redshift Distribution of Flat-Spectrum Radio Sources

J. A. Muñoz¹, E.E. Falco², C.S. Kochanek³, J. Lehár² and E. Mediavilla⁴

¹Departamento de Astronomía y Astrofísica, Universidad de Valencia, E-46100 Burjassot, Valencia, Spain

²F. L. Whipple Observatory, Smithsonian Institution, P. O. Box 97, Amado, AZ 85645, USA

³Harvard-Smithsonian Center for Astrophysics, 60 Garden St., Cambridge, MA 02138, USA

⁴Instituto de Astrofísica de Canarias, E-38200 La Laguna, Tenerife, Spain
email: jmunoz@uv.es

ABSTRACT

The redshift distribution of flat-spectrum radio sources with 5 GHz flux densities $S_5 \gtrsim 5$ mJy is a key component in using current radio lens surveys to probe the cosmological model. We have constructed the first flat-spectrum radio sample in the flux density range 3–20 mJy. Our new sample has 33 sources; we have determined the redshifts of 14 of these (42% complete). The low mean redshift, $\langle z \rangle \simeq 0.75$, of our faintest sample needs to be confirmed by further observations to improve the sample completeness. We also increased the redshift completeness of several surveys of brighter flat-spectrum sources. While the mean redshift, $\langle z \rangle \simeq 1.1$ of flat-spectrum samples fainter than 1 Jy is nearly constant, the fraction of the sources identifiable as quasars steadily drops from $\sim 80\%$ to $\sim 10\%$ as the flux density of the sources decreases.

Subject headings: cosmology: observations — galaxies: distances and redshifts — gravitational lensing — radio continuum: galaxies

1. Introduction

Imaging surveys of flat-spectrum radio sources have been the most successful systematic programs for discovering multiply imaged gravitational lenses. The JVAs (Patnaik et al. 1992, Browne et al. 1998, Wilkinson et al. 1998, King et al. 1999), CLASS (Browne et al. 2001, Myers et al. 2001, Chae et al. 2002) and PMNLS (PMN-based lensing survey) (Winn et al. 2000, 2002a, 2002b) surveys have discovered around 25 lenses to date, at a

rate of approximately 1 lens per 600 sources. Since the targets are selected from flux-limited catalogs of sources found in low resolution single-dish observations and the radio properties of a lens are unaffected by the optical properties of the lens galaxy or extinction in the lens galaxy, the radio lens samples avoid many of the possible statistical biases in samples of lensed quasars.

Unfortunately, the radio surveys also examine sources whose intrinsic redshift distributions are poorly constrained, and statistical models of lens samples depend strongly on the redshift distribution. In particular, the optical depth to multiple imaging in a flat cosmology scales as $\tau \propto D_{OS}^3$ where D_{OS} is the comoving distance to the source (Fukugita & Turner 1991, see also e.g. Kochanek 1993, and Muñoz, Kochanek & Falco 1999), making the uncertainties in the redshift distribution an important source of systematic errors in using the statistics to estimate the cosmological model.

The three major flat-spectrum surveys, JVAS, CLASS and PMNLS, used 5 GHz flux density limits of $S_5 = 200$ mJy, 25 mJy and 60–80 mJy respectively. While complete redshift surveys were available for bright sources ($S_5 > 300$ mJy, e.g. CJI/CJII: Henstock et al. 1995; and the Parkes samples: Allington-Smith, Peacock & Dunlop 1991), accurate calculations of lensing statistics need the redshift distributions of sources with flux only 10% that of the survey limit because magnification pulls the lenses from fluxes below the survey limit into the sample. Kochanek (1996), in analyzing the JVAS survey, demonstrated that extrapolations of the flat-spectrum radio luminosity function to fainter fluxes left a strong degeneracy between the mean redshift of the fainter sources and the cosmological model. To address this problem, Falco, Kochanek & Muñoz (1998, hereafter FKM) began a program to systematically estimate the redshift distributions of fainter flat-spectrum sources. The initial survey considered samples of sources in three flux density ranges, 50–100 mJy, 100–200 mJy, and 200–250 mJy, with 45, 63 and 69 sources per sample and redshift completenesses of 58%, 68% and 80% respectively. Using these new measurements to constrain the flat-spectrum radio-luminosity function, FKM analyzed the statistics of the JVAS lens sample to find limits of $\Omega_0 > 0.27$ at $2-\sigma$ ($0.47 < \Omega_0 < 1.38$ at $1-\sigma$), for flat cosmological models with $\lambda_0 \neq 0$. FKM showed that reconciling optical and radio lens surveys required corrections for extinction in the optical surveys.

The newer and larger CLASS and PMNLS surveys have still fainter flux density limits of $S_5 > 25$ mJy, which means that their analysis requires the redshift distribution of sources with flux densities as low as $S_5 \approx 3$ mJy. Here we extend our redshift surveys of flat-spectrum radio sources toward these fainter flux densities. In §2 we present updated results for the three samples from FKM, each of which is now 80% complete. We also define a sample with flux densities from 20–50 mJy and present initial results on its redshift

distribution. In §3 we construct a sample of flat-spectrum radio sources with 5 GHz flux density of 3–20 mJy and describe the initial results for its redshift distribution. In §4 we discuss the results and their implications for cosmology.

2. Sample Definition and Status

We divide our discussion of the samples into two sections. The first section updates the three brighter samples from FKM and defines two fainter samples with 5 GHz flux densities of 20–50 mJy. The next two sections discuss the construction of a sample of fainter flat-spectrum sources. These fainter samples must be treated differently because there is no 5 GHz survey from which to select targets with flux densities of 3–20 mJy.

2.1. Samples With Fluxes Above $S_5 = 20$ mJy

For sources brighter than $S_5 = 50$ mJy we can start from the flat-spectrum sources in the JVAS and MIT-Greenbank (MG; Burke, Lehár & Conner 1992) lens surveys. FKM selected samples of 69, 63, and 45 sources with 5 GHz flux densities between 200–250 mJy, 100–200 mJy, and 50–100 mJy from the JVAS, MG, and MG surveys respectively. The samples consisted of all sources inside the flux range with a survey region set by the epoch of the main optical spectroscopy run. I-band optical images were obtained for identification and spectra were obtained with the MMT. We subsequently defined two additional samples of flat-spectrum sources with flux density ranges of 20–30 mJy and 30–50 mJy by combining the GB6 catalog (Gregory et al. 1996) with the NVSS catalog (Condon et al. 1996). Tables 1–5 present these 5 samples with the estimated I-band magnitudes and the current redshift measurements, the emission and/or absorption lines identified and the “type” or classification of the objects. We have classified the objects only taking into account spectral characteristics: quasar (Q) for objects showing broad emission lines, BL Lac (b) for objects with only weak absorption lines but no emission lines, late-type galaxies (L) when only narrow emission lines are present and early-type galaxies (E) for spectra without emission features. We also have labeled as detected (D) objects with very low signal-to-noise ratio spectra where we found no emission or absorption lines. Because any broad emission line would have been easily detected on the D-type objects, we assume that they are radio-galaxies rather than quasars. In addition we have labeled the quasars as having relatively narrow absorption lines (N) and broad absorption lines (B). All three brighter samples (Tables 1, 2 & 3) from FKM are now 80% complete, while the two new, fainter samples (Tables 4 & 5) are only 15% complete. Figure 1 shows the histogram of redshifts

as in FKM for the 3 brighter samples and for the VLA sample (see below). Marlow et al. (2000) have measured 64% of the redshifts in a sample of 42 flat-spectrum sources with 5 GHz flux densities of 25–50 mJy; we rely on their results in this flux density range.

3. Selecting a Fainter Sample: VLA Observations

Down to a flux density limit of about 20 mJy we can obtain samples of flat-spectrum sources by combining the GB6 catalog (Gregory et al. 1996) with the NVSS (Condon et al. 1996), but at flux densities below 20 mJy, there is no complete 5 GHz survey that we can use to define a flat-spectrum sample (GB6 reaches 15 mJy in certain areas, but biases would encroach). We have built a catalog of faint flat-spectrum radiosources with 5 GHz flux densities of 3 to 20 mJy by conducting a 5 GHz VLA snapshot survey of NVSS sources which might have 1.4 GHz flux densities in this range if they were flat-spectrum sources.

If $S_\nu \propto \nu^\alpha$, we define flat-spectrum sources as those with spectral indices $\alpha > -0.5$ between 1.4 GHz and 5 GHz. While most flat-spectrum sources have $-0.5 < \alpha < 0.5$, there is a small tail out to $\alpha \sim 2$. Thus, most flat-spectrum sources with flux densities of 10–20 mJy will have 1.4 GHz flux densities of 5–50 mJy. However, the relatively rare sources with $0.5 < \alpha < 2$ could have 1.4 GHz flux densities of only 0.5–5 mJy. Based on these expectations, we obtained 200 snapshots of “bright” 5–50 mJy NVSS sources and 100 snapshots of “faint” 2–5 mJy NVSS sources to construct a reasonably fair sample of about 50 flat-spectrum sources with 3–20 mJy flux densities at 5 GHz.

We obtained the 6 cm snapshots using the VLA in the C array (program AL467 on 1998.12.08 and 1998.12.10). We chose the C array to ensure that most of the extended structure was captured, while still obtaining some information on the source morphologies. To reduce our VLA survey to fit in a reasonable observing schedule, we narrowed our DEC range to $25^\circ \pm 1^\circ$ and used only the northern sample RA= $8^h \rightarrow 16^h$ (1950), that was also covered by the FIRST survey (Becker, White & Helfand 1995). Our 6 cm C-array maps should scale well with the 20 cm B-array FIRST maps, permitting detailed spectral index determinations of the individual radio components. Integration times were 3 min (5 min) per target for the 200 “bright” (100 “faint”) targets. We applied standard VLA calibration techniques using observations of phase calibrators at intervals of ~ 15 min, and an assumed flux density for 3C286 of ≈ 7.5 Jy. The resulting data were self-calibrated and mapped, yielding images, each with an angular resolution of $4''$ and covering field of $\sim 8'$. The off-source RMS noise levels were ~ 0.13 and ~ 0.073 mJy/beam for the “bright” and “faint” target maps, respectively.

For each target, the maps were visually inspected and photometric boxes were defined to enclose each radio component. We assigned a morphology code as follows: “P” indicates a point source; “G” is for part of a lobed radio galaxy; “Q” is for an anomalous morphology; and “F” is for an unclassifiable faint source. The VLA observations failed to detect 14 of the “bright”, and 24 of the “faint” targets. These non-detections should all be steep-spectrum sources. The JVAS, CLASS and PMNLS surveys were originally selected based on 6 cm and 20 cm single-dish observations and could simply use ratios of the observed flux densities to determine the spectral index. While the NVSS survey resolution is sufficiently low to mimic single dish observations, our 6 cm VLA observations are not. A spectral index defined simply by the ratio of the NVSS and VLA flux densities will be biased towards a steeper spectral index because the VLA observations may resolve out some of the 6 cm flux density. To account for this we used the FIRST survey, whose angular resolution closely matches that of our VLA observations, to estimate a corrected spectral index. We used the NVSS/FIRST flux density ratio to estimate the flux density of any extended structure at 20cm, and then extrapolated its contribution to the 6cm flux density assuming a spectral index of -1 . Adding this to the flux density measured with the VLA gives us a corrected 6cm flux density (“corr” in Table 6). We then computed a spectral index between the corrected 6 cm and NVSS flux densities. Figure 2 shows the distribution of spectral index against corrected 6 cm flux density for all of our targets (in grey). Those sources with corrected 6 cm flux densities in the range $3 \rightarrow 20$ mJy and a spectral index flatter than -0.5 were selected for optical follow-up. The resulting sample of 33 sources, presented in Table 6 and shown in Figure 2 (black), covers the flux density range below the CLASS detection limit. It is clear that without including the “faint” targets, our spectral index distribution would have been biased at fainter 6 cm flux densities. The spectral index and flux density distribution of the sources will not be a perfect match to a survey starting from a complete 5 GHz catalog, but it should be reasonably close.

3.1. Optical Follow up

We followed the same procedures as in FKM. We first obtained I-band images for each radio source at the Fred Lawrence Whipple Observatory (FLWO) 1.2 m telescope. The detector was the 4SHOOTER camera; it employs 4 edge-buttable, thinned and AR coated Loral CCD’s. These chips have a 2048×2048 format with 15-micron pixels. At the focal plane, these map into 0.666 arcsec (binned 2×2). Our targets were centered on chip 3, which has a gain of 3.8 electrons per ADU and a readout noise of 9 electrons/pixel. We acquired up to three 30-minute exposures for each target, but 10 sources remained undetected in the combined images, implying they were fainter than $I \gtrsim 22 - 23$ mag.

The magnitudes (see Table 7) were calibrated using only the measured magnitude of a few unsaturated GSC stars serendipitously found in our fields, assuming $V - I = 1$ mag for them. We were concerned only with identifying the sources and estimating the likelihood of obtaining a redshift rather than in obtaining very accurate photometry. Moreover, most of the observations were carried out in non-photometric conditions; thus, accurate calibration was not possible in many cases.

For each of the 23 optically identified radiosources we acquired a spectrum with the 4.2m William Herschel Telescope at the Canary island of La Palma (Spain). We used the medium-resolution spectrograph ISIS with a dichroic slide permitting simultaneous observations in both blue and red channels. The detectors were a thinned EEV12-type ($4k \times 2k$) device on the blue arm with grating R300B covering the wavelength interval $\sim 3000\text{-}5500 \text{ \AA}$ with a dispersion of 0.86 \AA/pixel , and a TEK CCD ($1k \times 1k$) on the red channel with grating R158R covering the wavelength interval $\sim 5500\text{-}8500 \text{ \AA}$ with a dispersion of 2.90 \AA/pixel . The exposure times were typically 30 minutes; we combined 3 of these for the fainter objects. Despite the faintness of the objects, we unambiguously detected 19, or 83% of the optically identified objects. To determine the redshifts, we analyzed emission (absorption) line spectra with the IRAF¹ task EMSAO (XCSAO).

In Table 7 we show, for each object, the I-band magnitudes and redshifts obtained, the emission and/or absorption lines identified and the object classification as described in §2.1. Because of the faintness of the objects, correctly identifying the spectral features was a challenge. Of the 23 objects, we classified 5 only as “detected” (D-type, see §2.1) and 5 have only a tentative estimate (redshifts in parentheses). Of these 5, J0950+2434 and J1207+2530 had very noisy spectra; we used a tentative identification for the HK break to estimate the redshift. The continua of J0856+2426 and J1359+2516 were detected only near the noise level, but each spectrum contained a single narrow emission line that we tentatively identified with OII. Finally, J0904+2515 had a weak continuum plus a pair of relatively broad emission lines that we tentatively identify as Ly α and NeV. Including the tentative redshifts, the completeness of the redshift measurements is 42%.

¹IRAF is distributed by the National Optical Astronomy Observatories, which are operated by the Association of Universities for Research in Astronomy, Inc., under contract with the National Science Foundation.

4. Discussion

The most striking feature in the evolution of the flat-spectrum source population is the rapidly declining fraction of quasars for 5 GHz flux densities below 1 Jy, as shown in Figure 3. FKM had already noted this feature, but the interpretation depended on the assumption that systems for which they failed to measure redshifts were likely to have the spectra of galaxies rather than quasars. Our measurements of additional redshifts largely confirm this assumption. With a completeness above 80% we found that at ~ 1 Jy the quasar population is approximately 80%, however at ~ 100 mJy it is only $\sim 55\%$. If the assumption also holds for our fainter samples, the fraction of flat spectrum sources that are quasars drops from $\sim 80\%$ at 1 Jy to only $\sim 10\%$ at 10 mJy. However, because we find a plateau in the quasar fraction for the radio flux density between 50 and 250 mJy, greater completeness is needed in the faintest samples to understand the radio source population at these faintest radio flux densities. The FKM models for the radio luminosity function, as earlier studies by Dunlop & Peacock (1990), treated the flat-spectrum sources as a single population. Clearly, any new estimate will need to divide the flat-spectrum sources into two populations, “quasars” and “galaxies”, where the quasars have higher average radio luminosities and redshifts (and hence fluxes) than the galaxies.

FKM also noted that the average source redshift was nearly constant in the fainter samples. Figure 4 shows the mean redshift of the samples as a function of flux density. The low completeness of the two faintest samples (ours and Marlow et al. 2000) makes the interpretation tentative, but the average of the measured redshifts is declining in the faintest sample. The ease of measuring redshifts probably means that we first measure the redshifts of all quasars, and then slowly measure the redshifts of the galaxies starting at lower redshifts where the galaxies will tend to be brighter. This will generally mean that when quasars dominate the sample, completing the redshift measurements will reduce the mean redshift, but that when galaxies dominate the sample, completing the redshift measurements will raise the mean redshift.

In deriving cosmological limits from the statistics of the radio lens surveys, FKM considered 3 models for the distribution of unmeasured redshifts in the redshift surveys of flat-spectrum sources (see also Kochanek 1996 for details about the radio luminosity function model construction). Case A assumed the completeness was independent of redshift, case B assumed that completeness declined linearly with increasing redshift, and case C assumed that it increased linearly with increasing redshift. Case B (Case C) implies higher (lower) average source redshifts leading to lower (higher) estimates of the matter density Ω_m for a given number of lenses. It appears from Figure 4 that even the conservative Case C estimate for the completeness may have overestimated the mean redshift of the radio

sources, perhaps explaining why the FKM cosmological limits marginally disagree with more popular estimates (e.g., Riess et al. 1998; Perlmutter et al. 1999). The completeness models used by FKM do not represent a good model for the data described as galaxies versus quasars; but, new models for the flat-spectrum radio luminosity function should be based on more complete redshift samples.

Table 8 summarizes the current status of the project providing for each sample the total number of sources, total number of sources spectroscopically identified, number of quasars, number of galaxies, number of sources with a spectroscopy detection but not a redshift determination (these objects named “detected” are probably galaxies rather than quasars), completeness in the measured redshifts, mean redshift and the standard deviation in the redshift distribution (for the total sample and split between quasars and galaxies). If the lower average redshift of our 3–20 mJy sample is not simply an artifact of either the sample or the completeness of our redshift measurements, then it is an important component necessary to revise the statistics of radio-selected lenses. In particular, it would mean that surveys of fainter radio sources for lenses would have reduced yields because of the lower average source redshift.

Acknowledgments: The William Herschel Telescope is operated on La Palma by the Isaac Newton Group (ING) of Telescopes in the Spanish Observatory Roque de los Muchachos of the Instituto de Astrofísica de Canarias (IAC). Based also on observations obtained at the Multiple Mirror Telescope Observatory, a facility operated jointly by the University of Arizona and the Smithsonian Institution. JAM is a *Ramón y Cajal Fellow* from the *Ministerio de Ciencia y Tecnología* of Spain. EEF, CSK and JL were supported in part by the Smithsonian Institution.

REFERENCES

- Allington-Smith, J. R., Peacock, J. A., & Dunlop, J. S. 1991, MNRAS, 253, 287
- Browne, I. W. A., Wilkinson, P. N., Patnaik, A. R., & Wrobel, J. M. 1998, MNRAS, 293, 257
- Browne, I. W. A. & The Class Collaboration 2001, ASP Conf. Ser. 237: Gravitational Lensing: Recent Progress and Future Go, 15
- Becker, R. H., White, R. L., & Helfand, D. J. 1995, ApJ, 450, 559
- Burke, B. F., Lehàr, J., & Conner, S. R. 1992, Gravitational Lenses, Proceedings of a Conference Held in Hamburg, Germany, 9-13 September 1991. Edited by Rainer

- Kayser, Thomas Schramm, and Lars Nieser. Springer-Verlag Berlin Heidelberg New York. Also Lecture Notes in Physics, volume 406, 1992, p.237, 237
- Chae, K.-H. et al. 2002, Phys. Rev. Lett., in press, astro-ph/0209602
- Condon, J. J., Cotton, W. D., Greisen, E. W., Yin, Q. F., Perley, R. A., & Broderick, J. J. 1996, Astronomy Data Image Library, 01
- Dunlop, J. S. & Peacock, J. A. 1990, MNRAS, 247, 19
- Gregory, P. C., Scott, W. K., Douglas, K., & Condon, J. J. 1996, ApJS, 103, 427
- Falco, E. E., Kochanek, C. S., & Muñoz, J. A. 1998, ApJ, 494, 47, FKM
- Fukugita, M., & Turner, E.L., 1991, MNRAS, 253, 99
- Henstock, D. R., Browne, I. W. A., Wilkinson, P. N., Taylor, G. B., Vermeulen, R. C., Pearson, T. J., & Readhead, A. C. S. 1995, ApJS, 100, 1
- King, L. J., Browne, I. W. A., Marlow, D. R., Patnaik, A. R., & Wilkinson, P. N. 1999, MNRAS, 307, 225
- Kochanek, C. S. 1993, MNRAS, 261, 453
- Kochanek, C. S. 1996, ApJ, 473, 595
- Myers, S. T. & The Class Collaboration 2001, ASP Conf. Ser. 237: Gravitational Lensing: Recent Progress and Future Go, 51
- Muñoz, J. A., Kochanek, C. S., & Falco, E. E. 1999, ApJ, 521, L17
- Patnaik, A. R., Browne, I. W. A., Walsh, D., Chaffee, F. H., & Foltz, C. B. 1992, MNRAS, 259, 1P
- Perlmutter, S. et al. 1999, ApJ, 517, 565
- Riess, A. G. et al. 1998, AJ, 116, 1009
- Wilkinson, P. N., Browne, I. W. A., Patnaik, A. R., Wrobel, J. M., & Sorathia, B. 1998, MNRAS, 300, 790
- Winn, J. N. et al. 2000, AJ, 120, 2868
- Winn, J. N., Lovell, J. E. J., Chen, H., Fletcher, A. ;, Hewitt, J. N., Patnaik, A. R., & Schechter, P. L. 2002a, ApJ, 564, 143

Winn, J. N. et al. 2002b, AJ, 123, 10

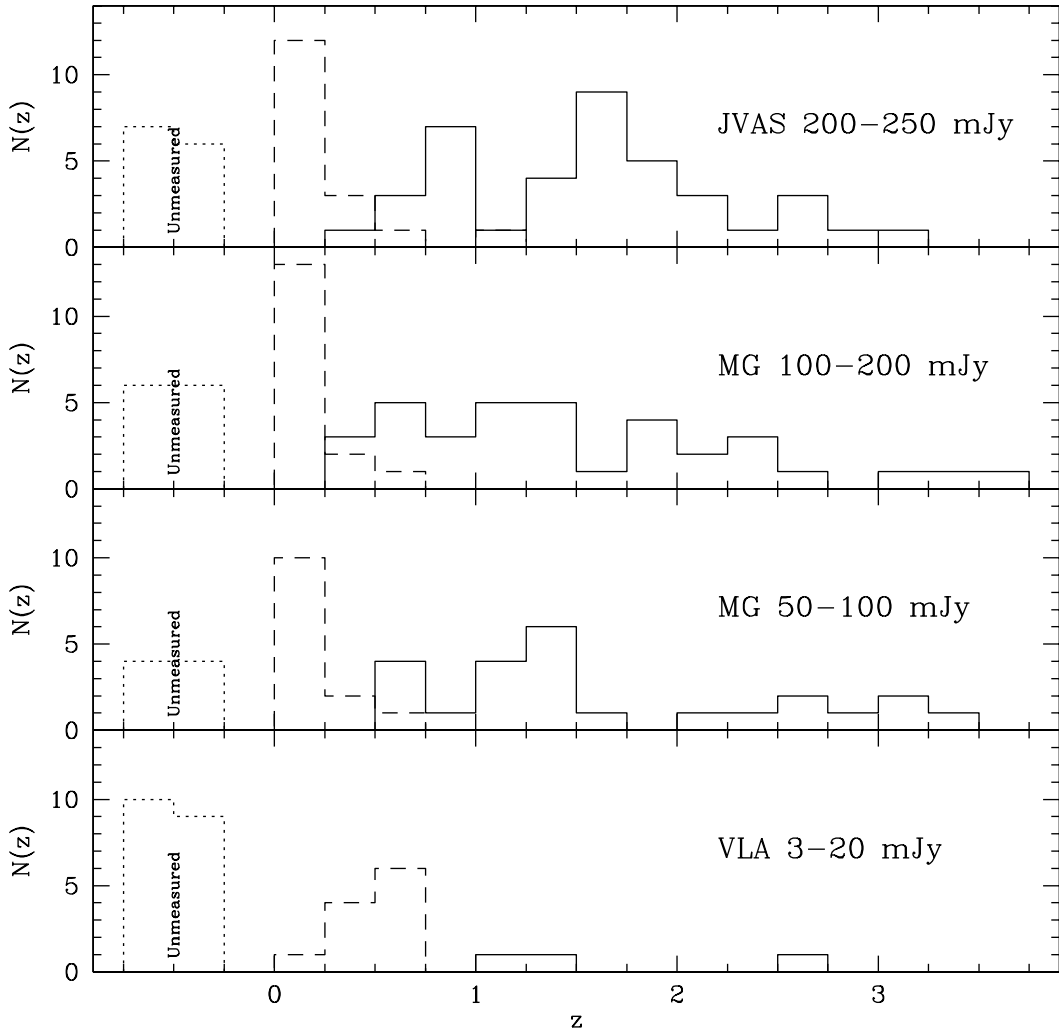


Fig. 1.— Histograms of redshifts for galaxies (dashed lines) and quasars (solid lines) in the samples JVAS (200-250 mJy), MG(100-200 mJy), MG(50-100 mJy) and VLA (2-30 mJy). The histograms at negative redshifts show the numbers of objects with undetermined redshifts, note that the faintest sample has a very low redshift completeness.

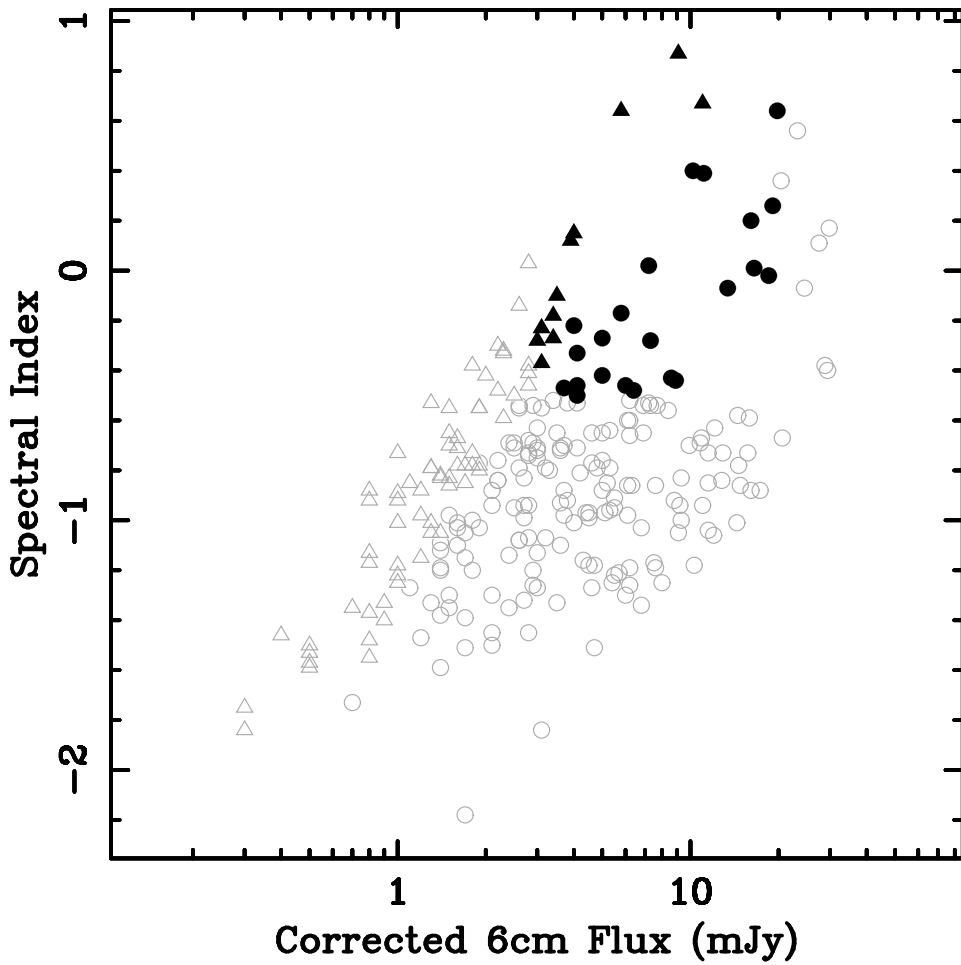


Fig. 2.— Distribution of source spectral index versus corrected 6 cm flux density. Spectral indices are determined using 20 cm flux densities from NVSS. Triangles (circles) indicate targets in the “faint” (“bright”) sample, and black symbols show those selected for optical follow-up.

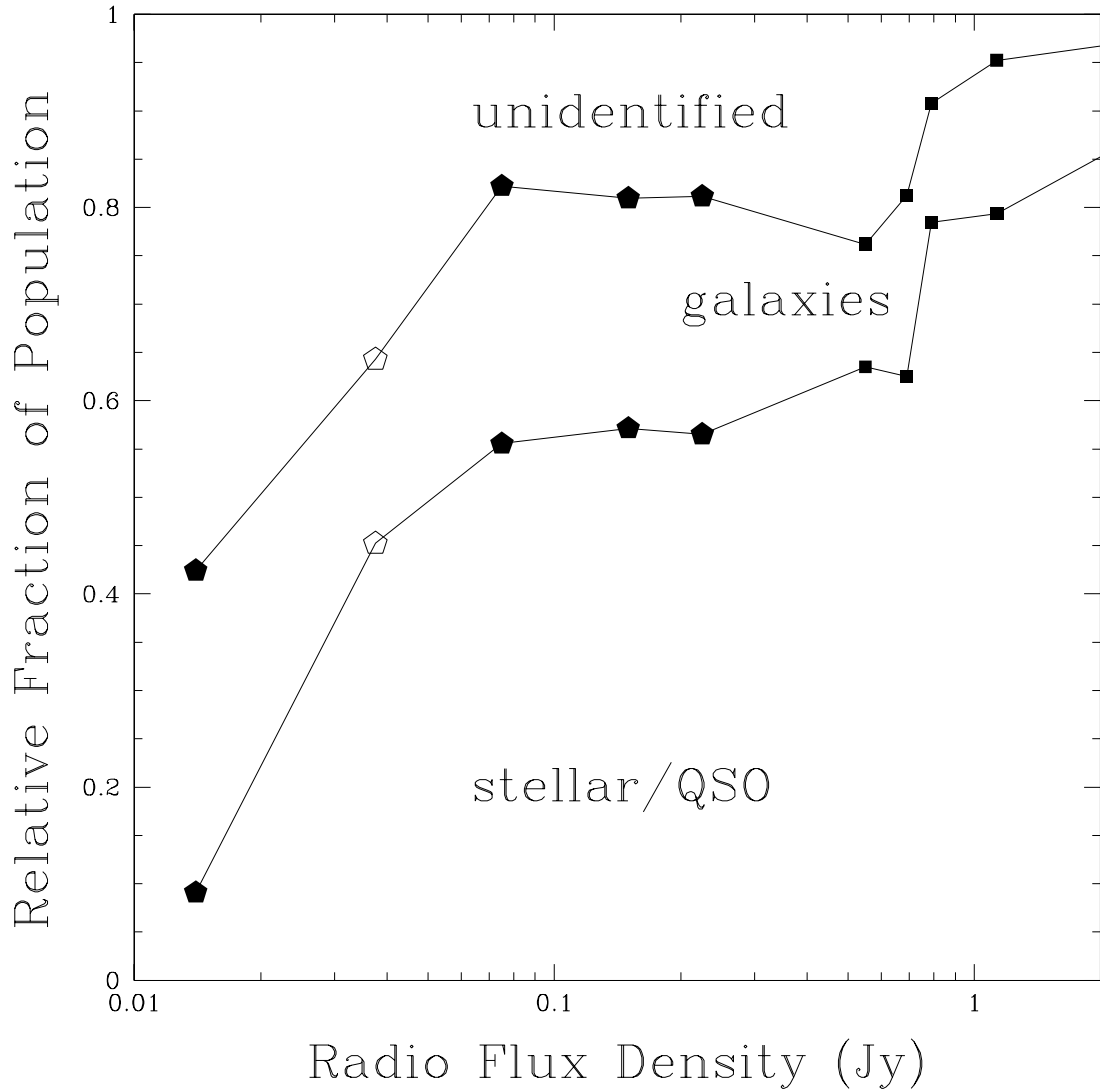


Fig. 3.— Relative population fractions as a function of the radio flux density. The region below the lower solid line shows the fraction of spectrally identified quasars in the population. The region between the solid lines shows the fraction of spectrally identified galaxies in the population. The region above the upper solid line shows the fraction of objects without a spectroscopic identification. The filled squares are from the PHFS sample, the filled pentagons are our current results, the triangles are previous results for the same samples, and the open pentagons are from Marlow et al. (2000).

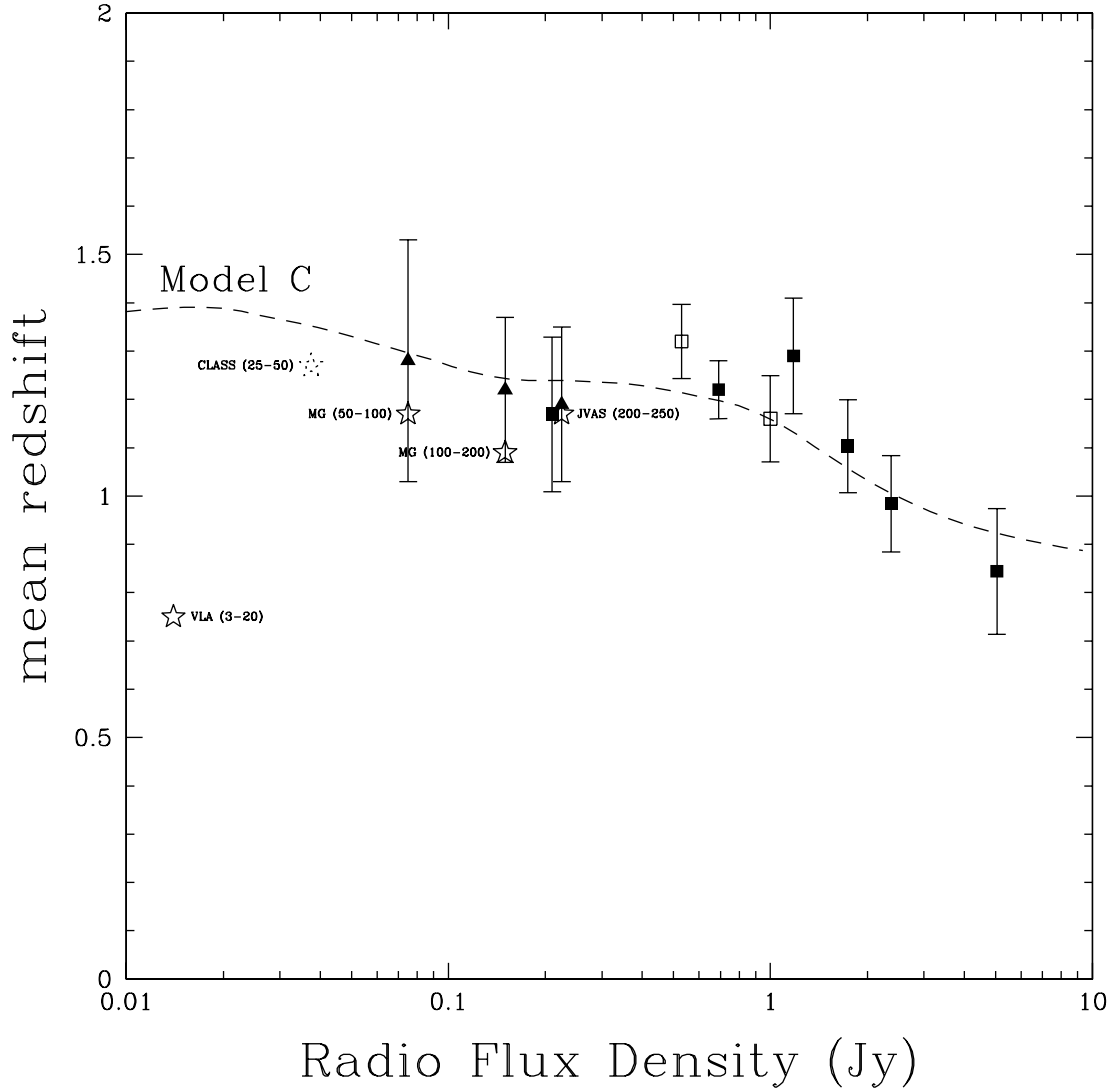


Fig. 4.— Mean redshift distribution as a function of the radio flux density. The points show the previous results from the Parkes samples (filled squares), Caltech-Jodrell I/II samples (open squares), and our old samples (triangles) along with the most conservative Case C model for the redshift distribution from FKM (dashed lines). The error bars are the dispersion of the redshift measurements. The Case C model assumed that redshift completeness rises linearly with source redshift. Superposed on these previous results are the new and updated results from this paper (stars) and the results from Marlow et al. (2000, dotted star). Note how even the Case C model seems to overestimate the average redshift distribution of the flat-spectrum sources.

Table 1. Sample 1 (JVAS 200–250 mJy)

Object	α (B1950)	δ (B1950)	I	σ_I	z	σ_z	type	detected lines
0902+468	09 02 52.68	46 48 21.71	14.8	0.2	0.0848	0.0005	L	(HK, H δ , G, Mg, CaFe, Na), H α , OIII
0903+669	09 03 01.85	66 56 51.58	18.9	0.2				
0905+420	09 05 20.99	42 02 56.14	18.2	0.1	0.7325	0.0008	Q	CIII], MgII, H γ , H β
0920+416	09 20 19.92	41 38 20.60	18.0	0.1	(0.07)	0.01	E	(HK, Mg, Na)
0924+732	09 24 51.83	73 17 12.42	18.6	0.1			D	
0927+469	09 27 17.71	46 57 20.96	16.8	0.2	2.032	0.001	Q	Ly α , SiIV, CIV, CIII]
0927+586	09 27 10.76	58 36 35.55	17.1	0.1	1.9645	0.0009	Q	Ly α , SiIV, CIV, HeII, CIII]
0939+620	09 39 29.44	62 04 17.76	18.0	0.2	0.7533	0.0005	Q	MgII, NeV
0951+422	09 51 06.97	42 15 20.74	19.3	0.1	1.783	0.004	Q	SiIV, CIV, CIII], MgII
0955+509	09 55 22.22	50 54 18.83	17.7	0.2	1.154	0.002	Q	CIV, CIII], CII, MgII, HeI
1010+495	10 10 20.75	49 33 33.83	18.5	0.1	2.201	0.002	Q	Ly α , CIV, CIII]
1023+747	10 23 13.02	74 43 44.02	17.5	0.2	0.879	0.002	Q	MgII, OIII, OIV
1027+749 [†]	10 27 13.30	74 57 23.11	15.2	0.2	0.123	0.001	E	
1028+564	10 28 50.61	56 26 23.42	21.5	0.5			D	
1101+609	11 01 50.75	60 55 07.10	18.9	0.2	1.363	0.003	Q	CIV, CIII], MgII
1109+350	11 09 55.21	35 02 58.82	19.1	0.2	1.9495	0.0003	Q	Ly α , CIV, CIII]
1116+603 [†]	11 16 19.23	60 21 22.49	17.5	0.2	2.638		Q	
1117+543	11 17 33.00	54 20 53.33	18.8	0.2	0.924	0.001	Q	CIII], MgII, OIIIa, NeV, H γ
1131+730	11 31 11.77	73 05 55.21	18.2	0.2	1.571	0.002	Q	SiIV, CIV, HeII, CIII], MgII
1147+438	11 47 39.81	43 48 47.00	18.8	0.1	3.037	0.008	N	Ly α , CIV, CIII]
1151+598	11 51 24.00	59 51 35.93	19.9	0.2	0.871	0.002	Q	CIII], MgII, H γ
1200+468	12 00 58.77	46 49 37.77	21.4	0.2				
1200+608	12 00 30.71	60 48 01.36	14.4	0.1	0.0656	0.0002	E	(HK, H δ , Mg, CaFe, Na)
1204+399	12 04 04.63	39 57 45.72	18.2	0.2	1.5134	0.0009	Q	CIV, CIII], CII, MgII
1231+507	12 31 27.08	50 42 54.89	16.7	0.1	0.2075	0.0005	E	(HK, G, Mg, CaFe Na)
1234+396	12 34 26.25	39 36 57.85	19.0	0.2			D	
1238+702	12 38 32.70	70 14 57.98	16.6	0.1	1.4706	0.0005	Q	CIV, CIII], MgII
1239+606	12 39 16.55	60 37 08.06	16.8	0.1	1.457	0.005	N	SiIV, CIV, NIII, CIII]
1245+676	12 45 32.18	67 39 38.12	16.9	0.2	0.1073	0.0002	E	(HK, H δ , G, H β , Mg, CaFe, Na)
1245+716	12 45 15.69	71 40 41.97	20.8	0.3			D	
1300+485	13 00 03.36	48 35 24.34	16.1	0.2	0.873	0.001	Q	CIII], CII, MgII, HeI
1300+693	13 00 50.97	69 18 57.72	17.1	0.2	0.5677	0.0003	L	CII, NeV, OII, HeI, H γ , OIII
1302+356	13 02 15.38	35 39 57.94	21.7	0.3				
1310+487	13 10 32.94	48 44 24.63	19.3	0.2	(0.313)	0.003	L	OIII, NeV, H γ , H β
1318+508	13 18 36.32	50 51 50.13	21.2	0.7			D	
1327+504	13 27 02.23	50 24 55.57	18.1	0.2	2.654	0.001	Q	OVI, SIV, Ly α , SiIV, CIV
1328+523	13 28 41.69	52 17 41.92	19.3	0.2			D	
1339+696	13 39 29.98	69 38 30.80	18.7	0.2	2.255	0.003	B	Ly α , CIV, CIII]
1341+691	13 41 42.19	69 10 21.11	17.3	0.2	1.417	0.002	Q	CIV, CIII], CII, MgII
1349+618	13 49 01.61	61 47 37.87	20.7	0.4	1.834	0.002	Q	CIV, NIII, CIII], NeIV
1409+595	14 09 49.22	59 31 08.20	20.1	0.2	1.725	0.009	Q	CIV, CIII], MgII
1412+461	14 12 19.18	46 08 46.22	19.9	0.2	(0.186)	0.002	E	(HK, H δ , CaFe, Na)
1418+375	14 17 55.81	37 35 18.25	17.9	0.1	0.969	0.002	B	NIII, CIII], MgII
1419+469	14 19 30.38	46 59 27.87	16.2	0.2	1.665	0.003	Q	SiIV, CIV, CIII], MgII
1421+511 [†]	14 21 28.55	51 09 12.34	15.0	0.2	0.274	0.002	Q	
1427+634	14 27 52.03	63 29 23.84	20.9	0.2	1.561	0.001	Q	CIV, HeII, CIII], CII, MgII
1438+501	14 38 04.29	50 10 56.24	17.7	0.2	(0.078)	0.001	E	(HK, H δ , G, Mg, Na)
1447+536	14 47 26.02	53 38 33.49	22.1	0.5				
1450+455 [†]	14 50 37.18	45 34 38.12	16.0	0.2	0.469		E	
1454+447	14 54 06.02	44 43 41.66	17.8	0.2				
1533+487	15 33 42.16	48 46 54.20	16.2	0.2	2.563	0.002	N	Ly α , CIV, CIII]
1556+745	15 56 54.94	74 29 32.56	19.3	0.2	1.667	0.001	Q	CIV, HeII, CIII], MgII

Table 1—Continued

Object	α (B1950)	δ (B1950)	I	σ_I	z	σ_z	type	detected lines
1557+565	15 57 41.57	56 33 41.87	16.0	0.1	(0.098)	0.001	E	(HK, G, H β , Mg)
1558+595	15 58 05.76	59 32 48.42	15.0	0.2	0.0602	0.0001	E	(HK, H δ , G, H β , Mg, CaFe, Na)
1603+573	16 03 34.72	57 22 42.20	16.3	0.2	0.720	0.001	Q	CIII], MgII, NeV, H γ , H β
1611+425	16 11 25.57	42 30 52.93	20.3	0.4				
1627+476	16 27 11.18	47 40 42.41	18.4	0.2	1.629	0.001	Q	SiIV, CIV, HeII, CIII], CII, MgII
1646+411	16 46 50.96	41 09 16.65	20.0	0.2	0.8508	0.0003	Q	CIII], MgII, H γ
1646+499	16 46 16.48	49 55 14.75	14.1	0.2	0.0475	0.0001	L	(HK, G, Mg, CaFe, Na), H α , OIII
1650+581	16 50 31.80	58 10 39.84	22.5	1.0				
1655+534	16 55 32.40	53 26 24.60	16.9	0.2	1.553	0.002	Q	CIV, CIII], MgII
1704+512	17 04 13.38	51 13 34.34	16.7	0.2	0.5303	0.0003	Q	MgII, NeV, HeI, OIII
1712+493	17 12 17.48	49 19 56.91	19.3	0.2	1.552	0.002	Q	CIV, HeII, CIII], MgII
1738+451	17 38 39.49	45 08 20.42	15.7	0.2	2.788	0.008	N	Ly α , CIV, CIII]
1742+378	17 42 05.62	37 49 08.35	16.4	0.2	1.9578	0.0005	Q	Ly α , SiIV, CIV, HeII, CIII]
1745+643 [†]	17 45 51.98	64 22 50.89	20.8	0.3	1.228		E	
1750+509	17 50 21.11	50 56 17.43	16.5	0.2	0.3284	0.0004	L	(HK, H δ , G, Mg, CaFe), Mg, OII, H γ , OIII
1752+356	17 52 27.92	35 41 17.64	16.8	0.2	2.207	0.002	Q	Ly α , CIV, CIII]
1755+626	17 55 23.68	62 37 03.36	15.1	0.4	0.0276	0.0001	E	(HK, H β , Mg, CaFe, Na)

Note. — A † indicates a previously known source as per NED, for which we did not obtain spectra; HK and G are the CaII H&K lines and G bands, respectively; parentheses surrounding a list of lines indicate absorption; parentheses surrounding a redshift indicate a marginal measurement; D, E, L, Q, B, N and b indicate respectively a detected object, an early-type galaxy, a late-type galaxy, a quasar, a quasar with broad absorption lines, a quasar with narrow absorption lines and a BL Lac object.

Table 2. Sample 2 (MG 100–200 mJy)

Object	α (B1950)	δ (B1950)	I	σ_I	z	σ_z	type	detected lines
MGC0001+2113	23 58 58.58	20 56 54.04	17.7	0.1	0.439	0.001	Q	NeIV, MgII, HeI, OIII
MGC0034+3712	00 32 14.32	36 55 53.66	18.9	0.2	1.390	0.002	Q	CIV, CIII], MgII
MGC0037+2613	00 34 40.35	25 56 43.50			0.1477	0.0002	E	(HK, G, H β , Mg)
MGC0042+2739	00 39 55.71	27 23 22.41						
MGC0046+2249	00 43 41.10	22 33 20.37			0.4312	0.0004	Q	MgII, NeV, HeI, H γ , H β , OIII
MGC0046+2456	00 43 28.10	24 40 09.40	17.1	0.2	0.7467	0.0004	Q	NeIV, MgII, HeI
MGC0054+2549	00 51 54.96	25 33 49.06						
MGC0054+3842	00 51 27.85	38 25 58.52			0.0622	0.0001	E	(HK, G, Hb, Mg, CaFe, Na), H α
MGB1606+2031	16 03 54.30	20 40 12.40	17.7	0.3				
MGB1634+1946	16 32 34.50	19 53 14.76	17.9	0.2	0.792	0.003	Q	CIII], CII, MgII, HeI
MGB1655+1949	16 53 32.99	19 53 29.07	19.0	0.2	3.260	0.003	N	Ly β , Ly α , SiIV, CIV
MGB1705+2215	17 03 22.21	22 20 08.25			0.04977	0.00008	E	(HK, G, H β , Mg, CaFe, Na)
MGB1715+3619	17 13 22.85	36 23 08.90	18.4	0.2	0.5549	0.0003	Q	MgII, HeI, H β , OIII
MGB1720+2334	17 18 05.64	23 38 29.12	17.4	0.2	1.852	0.003	Q	Ly α , SiIV, CIV, CIII], MgII
MGB1728+1931	17 26 44.62	19 33 31.38			0.1756	0.0003	E	(HK, G, H β , Mg, CaFe, Na)
MGB1745+2252	17 42 59.09	22 53 57.86	17.5	0.2	1.8838	0.0007	Q	Ly α , SiIV, CIV, HeII, CIII]
MGB1747+2323	17 45 45.21	23 25 37.51	17.1	0.1	2.203	0.002	N	Ly β , Ly α , SiIV, CIV
MGB1807+3107	18 05 38.33	31 05 52.75	18.3	0.2	0.5373	0.0004	N	MgII, NeV, OIII
MGB1813+3144 †	18 11 42.73	31 43 22.31	16.3	0.1	0.117		b	
MGB1834+2051	18 32 03.59	20 49 16.53	16.8	0.2	1.034	0.005	Q	CIII], MgII
MGB1835+2506	18 33 55.57	25 04 13.20			1.9728	0.0009	B	CIV, CIII]
MGB1843+3150	18 41 10.08	31 47 23.59	15.9	0.1	0.4477	0.0003	Q	MgII, NeV, HeI, H γ , H β
MGB1843+3225	18 41 37.21	32 22 22.47	19.6	0.3			D	
MGB1846+2036	18 43 55.22	20 32 54.81						
MGB1853+2344	18 51 22.48	23 40 48.28	17.2	0.2	1.0311	0.0008	Q	CIII], MgII
MGC2036+2227	20 34 44.58	22 17 29.07	16.4	0.1	2.567	0.002	Q	Ly α , SiIV, CIV, CIII]
MGB2043+2256	20 41 40.27	22 46 26.50	16.7	0.1	1.0810	0.0003	Q	CIII], MgII
MGB2051+1950	20 48 56.61	19 38 48.99	16.6	0.1	2.365	0.002	Q	Ly α , SiIV, CIV, CIII]
MGC2054+2407	20 52 17.47	23 56 05.77	19.6	0.2	1.3774	0.0005	Q	CIV, CIII], MgII
MGC2100+2058	20 57 49.45	20 47 34.81	17.6	0.1	(0.361)	0.001	E	(H δ , H β , CaFe, Na)
MGC2100+2346	20 57 51.93	23 35 17.88	17.0	0.2	1.124	0.001	Q	CIV, HeII, CIII], MgII
MGC2100+2615	20 58 28.63	26 03 49.70	20.0	0.4			D	
MGC2105+2920	21 03 35.78	29 08 49.82	18.6	0.1	1.347	0.002	Q	CIV, CIII], MgII
MGC2106+2135	21 03 55.28	21 23 31.85	17.8	0.1	0.6469	0.0008	Q	MgII, OII, OIII
MGC2109+2154	21 06 53.16	21 42 50.03	17.6	0.1	2.344	0.002	N	Ly α , CIV, CIII]
MGC2109+2211	21 07 40.17	22 00 00.30	18.4	0.1	2.281	0.002	Q	Ly α , CIV, CIII]
MGC2116+3016	21 13 59.43	30 04 05.38	17.3	0.2	2.080	0.003	N	Ly α , SiIV, CIV, HeII, CIII]
MGC2118+2006	21 16 08.43	19 54 54.12						
MGC2125+2441	21 23 11.64	24 29 00.28	18.0	0.5	(0.03)	0.01	E	HK, Mg, CaFe
MGC2130+3332	21 28 22.92	33 19 35.42	17.9	0.2	1.473	0.006	N	CIV, CIII], MgII
MGC2137+2357	21 34 49.60	23 43 31.15	17.1	0.2	0.6044	0.0007	Q	MgII, NeV, HeI, H γ , H β , OIII
MGC2153+2351	21 50 45.69	23 37 48.69						
MGC2203+3712	22 01 08.58	36 56 45.03	17.6	0.2	1.817	0.005	N	Ly α , CIV, MgII
MGC2213+2558	22 11 27.17	25 43 30.11	15.0	0.3	0.0940	0.0002	E	(HK, H δ , G, H β , Mg, CaFe, Na)
MGC2214+3550	22 12 44.73	35 36 29.15	18.2	0.2	0.877	0.003	Q	CIII], CII, MgII
MGC2214+3739	22 11 55.07	37 24 14.24						
MGC2223+2439	22 20 47.66	24 24 00.50	17.7	0.1	1.490	0.004	Q	SiIV, CIV, HeII, CIII], CII, MgII
MGC2227+3716	22 25 04.20	36 59 59.08	17.4	0.2	0.975	0.003	N	HeII, CIII], MgII, H γ
MGC2229+3057	22 27 15.93	30 41 48.78			0.3196	0.0004	L	NeV, HeI, H γ , H β , OIII
MGC2230+2752	22 27 55.30	27 38 18.77			(0.235)	0.001	E	(HK, H β , Mg, CaFe)
MGC2250+3825	22 47 48.11	38 08 42.70			0.1187	0.0003	E	(HK, G, H β , Mg, CaFe, Na)
MGC2251+2217	22 49 27.88	22 01 40.50	20.2	0.2	3.668	0.003	N	SIV, Ly α , CII, CIV

Table 2—Continued

Object	α (B1950)	δ (B1950)	I	σ_I	z	σ_z	type	detected lines
MGC2254+2058	22 52 27.05	20 42 36.60			0.0635	0.0002	E	(HK, H δ , G, H β , Mg, CaFe, Na)
MGC2257+3706	22 55 15.49	36 50 26.43						
MGC2301+3512	22 58 52.85	34 56 52.64			0.1357	0.0005	E	(HK, G, Mg, CaFe, Na), H α , OIII
MGC2308+2008	23 05 43.49	19 52 26.67			0.2342	0.0007	L	MgII, H β , OIII, H α
MGC2309+3726	23 06 51.15	37 09 53.28	19.2	0.2	(0.575)	0.001	E	(HK)
MGC2315+3727	23 12 44.93	37 10 32.86						
MGC2318+2404	23 16 05.73	23 48 14.79	17.2	0.1	1.054	0.002	Q	CIII], MgII, H δ
MGC2344+3433	23 42 20.80	34 17 09.05	17.8	0.2	3.053	0.007	B	SVI, Ly β , Ly α , CIV, CIII]
MGC2348+3539	23 46 27.36	35 23 19.46						
MGC2350+2331	23 47 43.12	23 15 19.61	19.1	0.2	1.693	0.001	Q	Ly α , SiIV, CIV, HeII, CIII], MgII
MGC2356+3840	23 54 26.73	38 23 33.25	18.5	0.2	0.2281	0.0003	E	(HK, G, Mg, Na)

Note. — See Table 1 for comments and definitions of object types.

Table 3. Sample 3 (MG 50–100 mJy)

Object	α (B1950)	δ (B1950)	I	σ_I	z	σ_z	type	detected lines
MG0803+3055	08 00 24.04	31 05 04.57	19.6	0.2	0.5618	0.0001	L	(HK), NeV, OII, HeI, H β , OIII
MG0809+3122	08 06 05.02	31 31 12.00	15.7	0.1	0.220	0.001	b	(HK, G, Mg, Na)
MG0814+2809	08 11 55.85	28 18 47.00	20.5	0.2	(0.138)	0.006	L	(HK, H δ , Na), OIII, H α
MG0828+2919	08 25 05.42	29 30 17.01	18.5	0.1	2.322	0.005	Q	OVI, Ly α , CIV, MgVII
MG0854+3009	08 51 31.15	30 21 24.85	21.6	0.3	(0.096)	0.001	L	H α
MG0909+2911	09 06 16.86	29 23 40.33	20.2	0.2	1.434	0.004	Q	CIV, CIII]
MG0920+2755	09 17 30.79	28 08 38.00	23.1	1.0			D	
MG0923+3059	09 20 07.97	31 12 18.00	17.2	0.1	0.6292	0.0006	Q	MgVII, MgII, NeV, HeI, H γ , H β
MG0926+2758	09 23 49.16	28 11 23.00						
MG0932+2837	09 29 18.29	28 50 47.00	17.6	0.1	0.3033	0.0002	E	(HK, H δ , G, H β , Mg, CaFe, Na)
MG0933+2844	09 30 41.39	28 58 52.00	18.3	0.2	3.428	0.002	N	Ly β , Ly α , SiIV, CIV
MG0940+3015	09 37 22.49	30 28 47.00	17.8	0.1	1.594	0.002	Q	SiIV, CIV, HeII, CIII], CII, MgII
MG1013+3042	10 10 15.13	30 58 25.00	18.4	0.1			D	
MG1019+3037	10 16 29.21	30 52 45.00	20.3	0.2	1.342	0.002	Q	CIV, HeII, CIII], MgVII, MgII
MG1023+2856	10 20 34.89	29 12 02.00	17.3	0.1	0.671	0.002	Q	CII, MgII, H γ
MG1028+3107	10 25 27.83	31 22 53.99	17.6	0.1	0.2403	0.0005	E	(HK, G, Mg, CaFe, Na), MgII, H α
MG1044+2958	10 41 19.77	30 14 46.00	18.0	0.1	2.981	0.001	Q	OVI, SIV, Ly α , SiIV, CIV
MG1045+3143	10 42 36.19	31 58 18.00	18.5	0.2	3.230	0.005	N	SIV, OVI, Ly α , SiIV, CIV
MG1106+3000	11 03 41.30	30 16 58.00	18.2	0.7				
MG1111+2841 †	11 08 31.45	28 58 05.00			0.02937	0.00003	E	
MG1112+2844	11 10 05.92	29 00 03.85	20.4	0.1			D	
MG1137+2935	11 34 43.15	29 52 15.00	17.7	0.2	2.644	0.001	N	OVI, Ly α , SiIV, CIV, HeII, CIII]
MG1142+2855	11 40 17.63	29 11 27.00			0.0974	0.0002	E	(HK, H δ , G, H β , Mg, CaFe, Na)
MG1145+2800	11 43 11.88	28 17 56.00	19.7	0.1	0.27	0.01	L	(HK, Mg), CII, OIII
MG1146+2845	11 44 11.73	29 01 22.00						
MG1202+2756 †	12 00 00.50	28 13 07.00	17.3	0.1	0.672		Q	
MG1213+2812	12 10 57.91	28 28 31.00	21.2	0.3			D	
MG1215+2750	12 13 18.26	28 06 16.00	16.6	0.2	0.1034	0.0001	E	(HK, G, H β , Mg, CaFe, Na)
MG1301+2822 †	12 58 55.76	28 37 44.00			1.373		Q	
MG1310+2925 †	13 07 43.24	29 42 15.00	18.0	0.2	1.21		Q	
MG1312+3113	13 10 27.54	31 28 53.00	16.6	0.1	1.0533	0.0009	Q	CIII], MgII, NeV
MG1334+3043	13 32 04.52	30 59 32.00	15.4	0.1	1.352	0.001	N	SiIV, CIV, NIII, CIII], MgII
MG1340+3009	13 38 24.62	30 23 43.00	17.4	0.1	2.197	0.002	Q	Ly α , SiIV, CIV, HeII, CIII], NeIV
MG1342+2828 †	13 40 36.25	28 43 10.00	17.5	0.1	1.037		Q	
MG1346+2900	13 44 20.21	29 15 40.00	20.3	0.2	2.721	0.003	Q	OVI, Ly α , SiIV, CIV
MG1347+2836 ‡	13 45 34.25	28 51 25.00	13.5	0.1	0.7407	0.0003	Q	MgII, NeV, OII, HeI
MG1353+2933	13 51 40.75	29 47 50.00	20.2	0.2	0.9714	0.0009	N	CIII], MgII, OII
MG1354+3139 †	13 51 51.20	31 53 45.00	17.8	0.1	1.326		Q	
MG1355+3023	13 53 26.22	30 38 51.00	18.2	0.1	1.0247	0.0007	Q	CIII], MgII
MG1356+2918	13 54 37.00	29 32 55.00	18.7	0.1	3.244	0.005	N	Ly α , SiIV, CIV
MG1400+2918	13 57 53.82	29 32 57.00	21.2	0.4	(0.164)	0.001	E	(HK)
MG1406+2930	14 03 56.65	29 45 58.00	20.7	0.2				
MG1415+2823	14 13 23.64	28 37 14.00	16.6	0.1	0.2243	0.0003	E	(HK, G, H β , Mg, Na)
MG1437+3119 †	14 35 31.49	31 31 57.00	17.8	0.1	1.366		Q	
MG1438+3001	14 35 49.42	30 15 03.00	16.9	0.2	0.2316	0.0003	E	(G, H β , Mg, CaFe, Na), MgII, NeV

Note. — See Table 1 for comments and definitions of object types. A \ddagger indicates likely contamination of the magnitude by a foreground star.

Table 4. Sample 4 (GB 30–50 mJy)

Object	α (J2000)	δ (J2000)	I	σ_I	z	σ_z	type	detected lines
GB1800+3137	18 00 06.18	+31 36 33.2						
GB1829+3139*	18 28 46.04	+31 38 08.9	16.3	0.1				
GB1852+2931	18 52 09.82	+29 31 00.7						
GB1902+3019	19 02 21.63	+30 19 04.2	14.9	0.2				
GB1934+2920	19 34 19.84	+29 20 07.4						
GB2028+2824*	20 28 08.93	+28 24 01.7	19.1	0.2				
GB2030+3106	20 30 07.30	+31 06 00.6						
GB2042+3034*	20 42 21.37	+30 33 50.7	17.5	0.2				
GB2045+3120	20 44 39.48	+31 20 04.1	18.7	0.2				
GB2060+2906	20 59 43.01	+29 05 41.9	19.5	0.2				
GB2109+3152	21 09 29.69	+31 52 11.7	17.2	0.4	0.0831	0.0002	E	(HK, G, Hb, Mg, CaFe, Na)
GB2114+3018	21 14 24.16	+30 17 53.2						
GB2116+3154*	21 16 15.11	+31 53 36.5	20.0	0.2				
GB2125+2930*	21 24 36.96	+29 30 28.1	15.9	0.2				
GB2138+3039*	21 37 55.66	+30 39 14.8	19.2	0.2				
GB2144+3134	21 44 15.23	+31 33 39.2	16.8	0.1			D	
GB2146+2852	21 46 14.43	+28 52 33.1	19.7	0.2				
GB2147+3103	21 47 22.21	+31 03 33.3	19.6	0.2				
GB2213+2910	22 13 18.12	+29 10 13.0	17.3	0.1	1.596	0.002	Q	CIV, HeII, CIII, MgII
GB2220+2814	22 20 28.71	+28 13 55.6	16.4	0.2				
GB2222+2836*	22 21 54.40	+28 35 58.8	18.2	0.1				
GB2241+2852	22 41 14.26	+28 52 19.7						
GB2250+2820	22 50 03.24	+28 19 58.0						
GB2301+3035	23 01 05.34	+30 34 11.0	15.8	0.3				
GB2303+3141	23 02 44.76	+31 41 34.0	20.1	0.2	2.79	0.01	N	Lyb, Ly α , SiIV, CIV, CIII
GB2307+3050	23 06 55.45	+30 50 28.2	20.3	0.4				
GB2330+2954*	23 29 44.57	+29 55 05.2	15.7	0.2				
GB2333+2802	23 32 50.34	+28 02 39.5	18.9	0.1				
GB2354+2931	23 53 58.62	+29 31 03.1	19.4	0.2				
GB2355+2855	23 54 59.05	+28 54 21.7	17.8	0.1				
GB2355+3151	23 55 20.61	+31 50 43.7	16.9	0.1				
GB2359+3021	23 59 19.30	+30 21 15.1	17.7	0.1				
GB0000+3056	00 00 10.10	+30 55 59.5	19.3	0.1	1.801	0.007	Q	SiIV, CIV, CIII, MgII
GB0004+3010	00 03 55.68	+30 10 03.1	19.7	0.2				
GB0010+2838	00 10 11.07	+28 38 12.4	18.7	0.1				
GB0010+2855	00 10 27.68	+28 54 58.3	20.0	0.2				
GB0039+2932	00 38 31.41	+29 32 20.7						
GB0102+3122*	01 01 35.09	+31 21 38.2	18.8	0.2				
GB0104+2805	01 03 35.50	+28 04 54.8						
GB0123+3102	01 23 12.33	+31 02 17.5	20.6	0.4				
GB0127+3118*	01 27 18.08	+31 17 58.9	19.8	0.2				
GB0135+2802	01 34 33.15	+28 02 08.8						
GB0149+2942	01 49 12.56	+29 42 30.5	16.8	0.1	0.340	0.001	Q?	MgII, OI, Hg, Hb, OIIIc, Ha
GB0150+3129	01 49 50.45	+31 28 56.5	18.4	0.1				
GB0152+2908	01 51 33.15	+29 07 38.3	19.4	0.1	1.402	0.005	Q	CIV, HeII, CIII, MgII
GB0153+2814	01 52 32.23	+28 13 22.3	19.1	0.1				
GB0211+3122	02 11 24.58	+31 22 03.3	16.6	0.1	1.001	0.005	Q	NIII, CIII, CII, MgII, HeI
GB0228+3032*	02 28 22.89	+30 31 48.0	19.4	0.4				
GB0233+3115	02 33 25.91	+31 15 01.1	20.4	0.2				
GB0233+3126	02 33 01.09	+31 25 33.7	19.0	0.1				
GB0234+2822	02 34 27.95	+28 22 21.8	19.3	0.2			D	
GB0234+2919	02 33 46.22	+29 18 52.8	19.9	0.2				
GB0245+2819	02 44 43.05	+28 19 08.5	16.2	0.2	0.1777	0.0002	E	HK, G, Hb, Mg, CaFe, Na

Table 4—Continued

Object	α (J2000)	δ (J2000)	I	σ_I	z	σ_z	type	detected lines

Note. — See Table 1 for comments and definitions of object types.

An asterisk indicates a hesitant optical identification from the I-band images (mainly due to the presence of several objects); the given I-band magnitude is tentative until the spectroscopic identification is performed.

A question mark next to the type of object indicates a tentative identification of the spectral features (see text for details).

Table 5. Sample 5 (GB 20–30 mJy)

Object	α (J2000)	δ (J2000)	I	σ_I	z	σ_z	type	detected lines
GB0801+3105	08 00 49.42	+31 04 36.4	19.0	0.2	1.739	0.001	Q	Ly α , CIV, HeII, CIII]
GB0806+2933*	08 05 59.28	+29 32 48.7	18.7	0.1				
GB0810+2957	08 10 05.34	+29 57 05.0						
GB0814+2941	08 14 21.24	+29 40 20.9	17.2	0.1				
GB0815+2850*	08 15 10.48	+28 49 51.3	16.0	0.2				
GB0820+3134	08 20 00.75	+31 34 10.5	15.6	0.2	2.324	0.005	Q	Ly α , SiIV, CIV, CIII]
GB0824+3132‡	08 23 36.26	+31 31 17.2	15.9	0.3	0.2160	0.0003	L	OII, HeI, H δ , H γ , H β , OIII], N1, H α , N2, S1, S2, (HK, M
GB0849+3160	08 48 50.95	+31 59 29.6	16.6	0.2				
GB0915+3021	09 14 42.72	+30 21 26.8						
GB0917+2950	09 16 37.52	+29 50 35.5						
GB0919+3118*	09 18 31.34	+31 18 36.7	15.9	0.1				
GB0933+2855	09 32 42.58	+28 54 49.7	16.0	0.2				
GB0938+2834	09 38 11.09	+28 33 57.1	19.7	0.2				
GB0938+3119	09 38 17.80	+31 18 53.7	20.4	0.3				
GB0942+2845	09 42 13.11	+28 45 12.2						
GB1020+2854	10 20 03.40	+28 53 28.0						
GB1021+3059	10 20 54.80	+30 59 30.0						
GB1022+3151	10 22 24.81	+31 50 59.1						
GB1029+3143	10 29 21.39	+31 42 12.1	15.5	0.2				
GB1031+2932	10 31 09.79	+29 32 00.1	21.2	0.7				
GB1032+2933	10 32 26.61	+29 32 32.5	16.2	0.2	1.290	0.002	Q	CIV, CIII], MgII
GB1033+2851	10 33 19.66	+28 51 21.0						
GB1044+3013	10 43 30.70	+30 12 53.0	16.8	0.2				
GB1055+3126	10 54 35.55	+31 25 49.5	16.2	0.2				
GB1056+2856	10 56 03.85	+28 56 14.3	15.8	0.3				
GB1056+3053	10 55 38.59	+30 52 54.8	16.7	0.2				
GB1106+2840	11 06 22.82	+28 40 02.9						
GB1112+3043	11 11 36.67	+30 43 06.1						
GB1118+3018	11 18 22.16	+30 18 02.7	20.1	0.2				
GB1121+2912	11 20 38.34	+29 11 59.6						
GB1124+2831†	11 24 29.65	+28 31 26.3	16.9	0.2	1.35		Q	
GB1132+3131	11 31 37.85	+31 31 21.9	16.9	0.3				
GB1152+2837	11 52 10.75	+28 37 20.9	16.0	0.2				
GB1204+2804	12 04 27.94	+28 03 22.3	16.1	0.2				
GB1204+3114	12 04 25.26	+31 13 27.5	15.7	0.2				
GB1206+2823	12 06 19.61	+28 22 54.4	15.6	0.2				
GB1208+3016	12 08 04.23	+30 15 50.7	18.7	0.1				
GB1213+3141†	12 13 20.00	+31 40 53.2	15.4	0.2	0.2065		G	
GB1216+2929*	12 16 27.58	+29 28 47.0	15.0	0.2				
GB1225+3118	12 25 14.97	+31 18 39.3	18.1	0.1				
GB1242+2851	12 41 35.14	+28 50 34.7	15.8	0.2				
GB1249+2927	12 48 58.75	+29 27 10.4	16.4	0.2				
GB1253+2857	12 53 07.64	+28 57 21.2	16.4	0.2				
GB1321+3137	13 21 12.82	+31 36 45.9	15.1	0.1				
GB1331+2932	13 31 01.78	+29 32 16.9	19.6	0.2				
GB1334+3015	13 34 14.32	+30 15 45.4	18.9	0.1				
GB1339+3060†	13 39 24.60	+30 59 27.3	14.4	0.2	0.0612		G	
GB1342+2939	13 41 36.34	+29 38 27.0	18.0	0.1	0.5302	0.0003	E	(HK, G, H β , Mg, CaFe)
GB1421+2916*	14 20 46.12	+29 15 56.2	19.8	0.2				
GB1515+3048	15 15 16.65	+30 47 30.2						
GB1608+3021	16 08 03.66	+30 20 29.3	18.9	0.6	0.65	0.05	E	(HK)
GB1613+2946	16 12 52.68	+29 45 30.7	19.8	0.2				
GB1626+2836*	16 26 07.81	+28 35 45.2	18.7	0.1				

Table 5—Continued

Object	α (J2000)	δ (J2000)	I	σ_I	z	σ_z	type	detected lines
GB1827+2839	18 26 31.74	+28 38 48.0	16.9	0.1	0.071		G	
GB1848+3107	18 47 37.68	+31 06 41.4	17.2	0.1				

Note. — See Table 1 for comments and definitions of object types.

An asterisk indicates a hesitant optical identification from the I-band images (mainly due to the presence of several objects); the given I-band magnitude is tentative until the spectroscopic identification is performed.

[‡]GB0824+3132 has a galaxy companion at the same redshift, with similar spectral features and separated only by ~ 2 arcsec.

Table 6. Sample 6 (VLA 3–20 mJy) – Radio properties

Object	α (J2000)	δ (J2000)	Mrf [†]	NVSS	First	VLA6	Corr	α
J0802+2513	08 02 56.78	+25 13 37.3	P	4.9±0.50	5.5±0.15	3.1±0.49	3.1±0.49	-0.37±0.19
J0824+2434	08 24 25.09	+24 34 28.4	F	4.1±0.50	3.7±0.18	3.3±0.47	3.4±0.48	-0.18±0.19
J0841+2440	08 41 46.76	+24 40 27.2	P	6.3±1.20	3.3±0.14	3.6±0.24	4.1±0.29	-0.46±0.20
J0844+2538	08 44 47.49	+25 38 24.5	F	11.5±1.00	10.6±0.29	6.3±1.05	6.4±1.07	-0.48±0.19
J0847+2518	08 47 20.71	+25 18 03.9	P	5.7±0.50	4.3±0.14	9.5±0.23	10.2±0.25	0.40±0.09
J0856+2426	08 56 50.46	+24 26 01.8	P	10.3±1.00	9.0±0.17	5.8±0.23	6.0±0.24	-0.46±0.10
J0857+2429	08 57 56.10	+24 29 22.6	P	2.7±0.50	1.8±0.13	8.3±0.19	9.1±0.26	0.87±0.19
J0904+2515	09 04 42.50	+25 15 38.0	P	8.9±0.50	13.8±0.16	19.8±0.25	19.8±0.25	0.64±0.06
J0909+2517	09 09 09.14	+25 17 38.4	P	3.8±0.60	2.7±0.15	2.9±0.19	3.1±0.21	-0.23±0.17
J0914+2510	09 14 00.33	+25 10 50.9	P	4.6±0.50	4.1±0.18	3.3±0.23	3.4±0.24	-0.27±0.13
J0916+2519	09 16 27.01	+25 19 43.6	P	18.8±0.70	18.5±0.14	18.4±0.22	18.5±0.22	-0.02±0.04
J0917+2532	09 17 14.16	+25 32 14.9	Q	12.6±0.60	49.8±0.18	16.1±0.32	16.1±0.32	0.20±0.05
J0926+2518	09 26 07.22	+25 18 45.1	P	7.7±0.50	9.1±0.16	4.1±0.18	4.1±0.18	-0.50±0.08
J0943+2430	09 43 28.25	+24 30 55.3	P	16.2±0.70	20.7±0.14	16.5±0.19	16.5±0.19	0.01±0.04
J0945+2526	09 45 06.54	+25 26 25.8	P	6.7±0.50	8.0±0.20	3.7±0.16	3.7±0.16	-0.47±0.09
J0950+2434	09 50 40.60	+24 33 48.6	P	3.3±0.50	3.7±0.16	4.0±0.25	4.0±0.25	0.15±0.16
J1016+2433	10 16 06.28	+24 33 16.1	P	6.0±0.50	2.5±0.15	5.0±0.17	5.8±0.22	-0.17±0.09
J1029+2418	10 29 23.93	+24 18 53.7	P	4.4±0.60	3.3±0.14	10.3±0.22	11.0±0.26	0.67±0.14
J1114+2433	11 14 59.17	+24 33 47.3	P	13.8±0.60	14.3±0.15	19.1±0.20	19.1±0.20	0.26±0.04
J1127+2530	11 27 47.01	+25 30 20.9	P	3.4±0.60	2.0±0.17	3.1±0.18	3.5±0.21	-0.10±0.19
J1129+2445	11 29 06.83	+24 45 23.7	P	4.1±0.60	3.6±0.18	2.9±0.17	3.0±0.18	-0.28±0.16
J1131+2459	11 31 49.12	+24 59 37.6	P	6.8±0.50	6.2±0.14	7.0±0.18	7.2±0.19	0.02±0.08
J1135+2457	11 35 45.80	+24 57 45.2	P	5.3±0.50	7.7±0.27	4.0±0.19	4.0±0.19	-0.22±0.11
J1148+2522	11 48 39.03	+25 22 19.8	P	8.5±0.50	12.7±0.16	5.0±0.23	5.0±0.23	-0.42±0.07
J1155+2435	11 55 59.05	+24 35 48.5	G	9.1±0.60	5.4±0.27	6.5±1.48	7.3±1.66	-0.28±0.24
J1201+2430	12 01 12.22	+24 30 28.1	P	6.7±0.50	5.8±0.14	4.8±0.19	5.0±0.20	-0.27±0.08
J1207+2530	12 07 28.79	+25 30 18.7	P	15.5±1.00	17.8±0.16	8.9±0.22	8.9±0.22	-0.44±0.07
J1223+2540	12 23 53.90	+25 40 02.5	P	14.6±0.60	14.9±0.14	13.4±0.21	13.4±0.21	-0.07±0.04
J1301+2521	13 01 29.44	+25 21 48.8	P	6.5±0.50	5.6±0.16	10.7±0.17	11.1±0.18	0.39±0.08
J1317+2426	13 17 43.01	+24 26 12.9	F	2.9±0.60	1.8±0.17	3.5±1.62	3.9±1.80	0.12±0.51
J1325+2459	13 25 10.21	+24 59 54.5	P	14.2±0.60	12.5±0.15	8.3±0.26	8.6±0.27	-0.43±0.05
J1359+2516	13 59 22.62	+25 16 18.6	P	2.6±0.50	3.2±0.15	5.8±0.22	5.8±0.22	0.64±0.20
J1500+2511	15 00 55.48	+25 10 54.0	F	5.5±0.50	3.3±0.18	3.7±1.52	4.1±1.69	-0.33±0.42

Note. — All flux densities are accumulated over all source components, and errors are r.m.s. uncertainties for the total flux density. Corrected 6 cm flux densities are adjusted to account for the excess of NVSS over FIRST flux, and the spectral index α is computed between the corrected 6 cm and NVSS flux densities.

[†]VLA morphology codes: P=point; G=part of a lobed galaxy; Q=quasi-point; F=faint.

Table 7. Sample 6 (VLA 3–20 mJy) – Optical properties

Object	<i>I</i>	σ_I	<i>z</i>	σ_z	type	detected lines
J0802+2513	23.23	1.60				
J0824+2434	18.11	0.02	0.3945	0.0007	E	(G, H β , Mg, CaFe, Na)
J0841+2440	20.65	0.12				
J0844+2538						
J0847+2518	18.45	0.02	0.5068	0.0007	L	OII, H β , OIII, (HK, G)
J0856+2426	19.90	0.07	(0.737)	(0.001)	L	OII??
J0857+2429	19.36	0.04	1.262	0.004	Q	CIV, CIII], MgII
J0904+2515	21.01	0.20	(2.66)	(0.01)	Q	Ly α , NeV ??
J0909+2517	21.13	0.16				
J0914+2510	18.13	0.02	0.327	0.001	E	(HK, G, H β , Mg, CaFe, Na)
J0916+2519	19.68	0.06	0.59	0.01	E	(HK)
J0917+2532	20.58	0.10			D	
J0926+2518						
J0943+2430	19.91	0.06			D	
J0945+2526	20.73	0.17			D	
J0950+2434	18.50	0.04	(0.50)	(0.01)	E	(HK, G)
J1016+2433	18.56	0.02	0.260	0.001	L	OII, OIII, (HK, Mg, CaFe, Na)
J1029+2418						
J1114+2433	21.67	0.30				
J1127+2530	20.85	0.17			D	
J1129+2445	16.21	0.01	0.1373	0.0004	E	(HK, G, Mg, CaFe, Na)
J1131+2459						
J1135+2457	20.37	0.10	0.691	0.001	E	(HK, G)
J1148+2522						
J1155+2435						
J1201+2430						
J1207+2530	19.25	0.04	(0.518)	(0.001)	E	(HK, G)
J1223+2540						
J1301+2521	18.69	0.03	1.186	0.003	Q	CIV, HeII, CIII], MgII
J1317+2426	19.63	0.08			D	
J1325+2459						
J1359+2516	20.59	0.14	(0.740)	(0.001)	L	OII?
J1500+2511						

Note. — See Table 1 for comments and definitions of object types.
A question mark next to the detected lines indicates a tentative identification of the spectral features (see text for details).

Table 8. Sample Properties

Sample	Source	Flux (mJy)	Objects	Ident.	QSO	Galaxy	Det.	Completeness (%)	\bar{z}	σ_z	\bar{z}_Q	σ_{z_Q}	\bar{z}_G	σ_{z_G}
1	JVAS	200–250	69	56	39	17	6	81	1.17	0.85	1.58	0.67	0.24	0.30
2	MG	100–200	63	51	35	16*	2	81	1.09	0.93	1.50	0.85	0.18	0.14
3	MG	50–100	45	37	24	13*	4	82	1.17	1.02	1.69	0.91	0.21	0.13
4	GB	30–50	53	8	7	1	2	15
5	GB	20–30	55	10	4	6	...	18
**	CLASS	25–50	42	27	19	8	...	64	1.27	0.95
6	VLA	3–20	33	14	3	11	5	42	0.75	0.63	1.70	0.83	0.49	0.20

Note. — *It includes one object tentatively identified as BL Lac. **Results from Marlow et al. (2000); their results supplement the low completeness of our 4 and 5 samples.